Chinese Chemical Letters 35 (2024) 109623

Contents lists available at ScienceDirect

Chinese Chemical Letters

journal homepage: www.elsevier.com/locate/cclet

Wettability-driven synergistic resistance of scale and oil on robust superamphiphobic coating

Yixuan Wang[a,b], Jiexin Li[a,b], Zhihao Shang[c], Chengcheng Feng[c], Jianmin Gu[c], Maosheng Ye[a,b], Ran Zhao[a,b], Danna Liu[a,b], Jingxin Meng[a,b,*], Shutao Wang[a,b]

[a] *CAS Key Laboratory of Bio-inspired Materials and Interfacial Science, Technical Institute of Physics and Chemistry, Chinese Academy of Sciences, Beijing 100190, China*
[b] *University of Chinese Academy of Sciences (UCAS), Beijing 100049, China*
[c] *State Key Laboratory of Metastable Materials Science and Technology (MMST), Yanshan University, Qinhuangdao 066004, China*

ARTICLE INFO

Article history:
Received 22 December 2023
Revised 30 January 2024
Accepted 7 February 2024
Available online 14 February 2024

Keywords:
Superamphiphobic
Durability
Wettability
Anti-scaling
Oil repellence

ABSTRACT

Disgusting deposits (*e.g.*, scale and crude oil) in daily life and industrial production are always serious problems, posing great threats to the safety and economic development. However, most of developed coatings can only conquer one part of these deposits such as superhydrophobic coatings possess anti-scaling capacity but would adhere crude oil. To integrate scale resistance with oil repellence, we herein report a robust superamphiphobic (SAB) coating simultaneously reducing pollution of scale and oil for extended period of time (two weeks with over 98% reduction). Compared with single role of superhydrophobic and amphiphilic surfaces, the SAB coating can not only inhibit interfacial nucleation of scale but also reduce the adhesion of formed scale and polluted oil. The durability of the SAB coating is evaluated *via* mechanical tests (sandpaper abrasion, tape stripping and sand falling) and chemical corrosion (corrosive liquid immersing), revealed by sustainable high contact angles and low contact angle hysteresis of water and oil. The universality of this strategy can be further confirmed by adding different particles like kaolin, Al_2O_3, and SiO_2, resisting multiple types of scale (*i.e.*, $CaSO_4$, $BaSO_4$ and $MgCO_3$) and oil (*i.e.*, glycerol, glycol, and mineral oil). Therefore, this study provides an ideal avenue for resisting scale and oil, which may be used for conquering the complexity of application environments (*e.g.*, oil production and transportation).

During the production of deep oil and gas, the amphiphilic (AL) pipeline surfaces are easily prone to scaling and waxing due to the high-salinity oil/water environment [1–3]. With time going by, the accumulation of these undesirable foreign deposits (*e.g.*, scale and wax) would sharply decline the productive efficiency and cause economic loss by blocking the transportation pipeline [4,5]. In order to solve these plugging problems, the advanced way is to modify the pipeline surface to prevent the depositions [6,7]. In recent years, superhydrophobic (SHB) and slippery surfaces have been employed for anti-fouling and anti-adhesion, obtaining fair efficiency and durability [8–14]. Most of these functional surfaces are usually oleophilic, which typically be used for oil/water separation, transport liquid and oil spill remediation [15–18]. However, this characteristic can easily be polluted by the oil from the high-salinity oil/water environment, following the problem of wax deposits [19–23]. This occurs because the wax usually precipitates from crude oil when temperature drops below the wax appearance temperature. In all, it is greatly significant to consider the actual operating environment and design the comprehensive anti-adhesion coatings.

Superamphiphobic (SAB) coating always possesses large contact angle (CA) and low contact angle hysteresis (CAH) for water (high surface tension) and oil (low surface tension), which have been widely used for self-cleaning, anti-wax, corrosion resistance, wearable sensors, liquid transportation and so on [24–30]. So this water/oil-proof performance can make it difficult for scale and wax adhesion on the surface. The unique properties mainly depend on two keys: hierarchical roughness and low surface energy. Currently, there exists increasing preparation methods including sol-gel synthesis, electrospinning techniques, chemical etching processes, and electrochemical anodization for fabricating the SAB coating [31–33]. Confronting the practical application, it is also vitally important to enhance the durability of the SAB coating like enhancing adhesion between the coating and substrate, developing self-

* Corresponding author.
E-mail address: mengjx628@mail.ipc.ac.cn (J. Meng).

https://doi.org/10.1016/j.cclet.2024.109623
1001-8417/

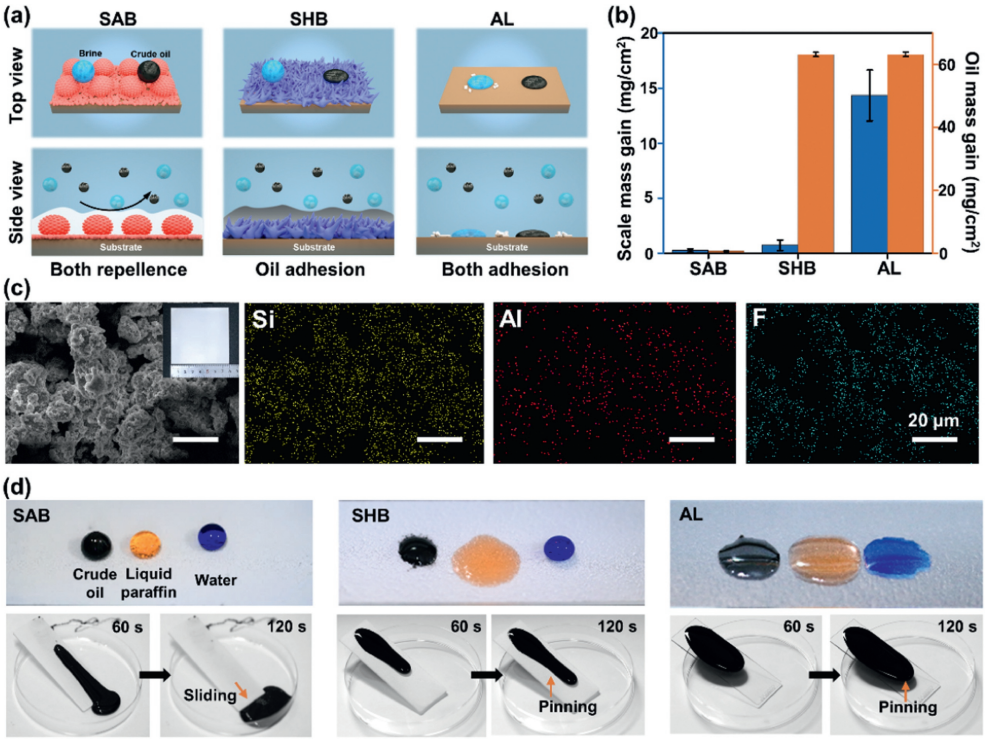

Fig. 1. The anti-adhesion properties of the SAB coating. (a, b) Scheme and graph illustrate that the SAB coating show the integrated scale and oil repellence performance compared with the SHB coating (oil adhesion) and AL surface (water and oil adhesion). (c) SEM and EDS images display the obtained SAB coating. The inset exhibits the photograph of the scalable SAB coating on an aluminum plate (8 cm × 8 cm). (d) The images demonstrate the state of liquid, like crude oil (black), liquid paraffin (dyed with Sudan IV) and water (dyed with methylene blue), and the flow process of crude oil on above-mentioned coatings.

healing materials and establishing multi-scale protective structures [34,35]. However, it is undeniable that every strategy has its own limitations. The adhesive coating may be destroyed beyond certain critical values and the healable materials need external stimuli and long time. In addition, the armored structures require complicated technology. Hence, it is essential to develop a simple way for constructing robust the SAB coatings.

As a natural silicate mineral, montmorillonite (MMT) with plate-like rough structure has the advantages of active surface groups such as -OH [36–38]. Hence, the MMT can be adopted as fillers owing to their facilitated surface modification and re-entrant structure for fabricating SAB coatings. Herein, we prepare a robust fluorinated-montmorillonite-based SAB coating on various substrates with synergistic scale and oil repellence by a facile spraying technology. The trapped air layer above SAB surface can keep the liquid droplets suspending on the top of the micro/nanostructures instead of penetrating into the micro/nanostructures due to the low surface energy (*ca.* 0.1 mN/m, Table S1 in Supporting information), resisting the approach of the scale and oil onto the surface (Figs. 1a and b). The SAB coating can achieve comprehensive and excellent scale and oil repellence performance for two-weeks test (*ca.* 98% reduction efficiency). The moderate surface energy of SHB surface (*ca.* 26.6 mN/m) can resist scale deposition while the oil can adhere on the substrate, leading to the accumulation of oil. The common AL surface (high surface energy of *ca.* 40.7 mN/m) would adhere to both much scale and oil. With this design, we regulated the hierarchical rough structure and low-surface-energy groups of the filler and polymer to adjust the morphology and wetting. Additionally, the SAB coating obtained on the metal net exhibited high stability and durability after mechanical damage and chemical corrosion (like sandpaper abrasion, tape stripping, sand falling and corrosive liquid immersing), which can be verified by the high CAs (> 150°) and low CAHs (< 2°) of water and oil. Moreover, this universality of this design can be proved from multi aspects by varying types of scale (*i.e.*, $CaSO_4$, $BaSO_4$ and $MgCO_3$), oil (*i.e.*, glycerol, glycol, and mineral oil) and additional particles (like kaolin, Al_2O_3, and SiO_2). Thus, we believe this work can provide valuable insights into anti-adhesion design toward real-world complex application environments.

As shown in Fig. S1 (Supporting information), the preparation of the SAB coating was depicted as previous reports [39]. Firstly, the suspension solution was obtained by mixing tetraethoxysilane (TEOS) and 1*H*,1*H*,2*H*,2*H*-perfluorodecyltriethoxysilan (PFDTES) in the presence of MMT nanoparticles. Then, SAB coatings were prepared by spraying the above-mentioned solution on different substrates (*e.g.*, glass, stainless steel, copper and metal mesh). The original MMT particles exhibited rough microstructures with abundant element of Al and Si rather than F as shown in Fig. S2 (Supporting information). Due to the junction from the ammonia-catalyzed hydrolytic condensation, the SAB coating showed a hierarchical micro/nanostructure displaying lots of F element (Fig. 1c). With the help of spraying method, the SAB coating can be deposited on various substrates in a large scale such as stainless steel shown in Fig. 1c inset. Compared with the original MMT, fluorinated-MMT (F-MMT) exhibited the stretching vibration peak of the C-F bond (1210 cm^{-1}) in Fig. S3a (Supporting information), resulting from the hydrolysis condensation of TEOS and PFDTES [34]. Moreover, the high-resolution C 1s spectrum in Fig. S3b (Supporting information) showed the peak of C–C (285.9 eV), CF_2 (291.9 eV) and CF_3 (294.1 eV), revealing the perfluorodecyl groups of the modified coatings [39]. The formation of excellent SAB coatings can be attributed to synergistic effect of the low surface energy and special re-entrant structure [40–42]. Especially shown in Fig. 1d, the crude oil, liquid paraffin (dyed with Sudan IV) and water (dyed with methylene blue) droplets revealed almost spherical on the SAB coating, verifying its repellence towards oil and water. More importantly, the crude oil was dumped on the SAB coating (with a tilt angle of *ca.* 20°) and the crude oil can slide down

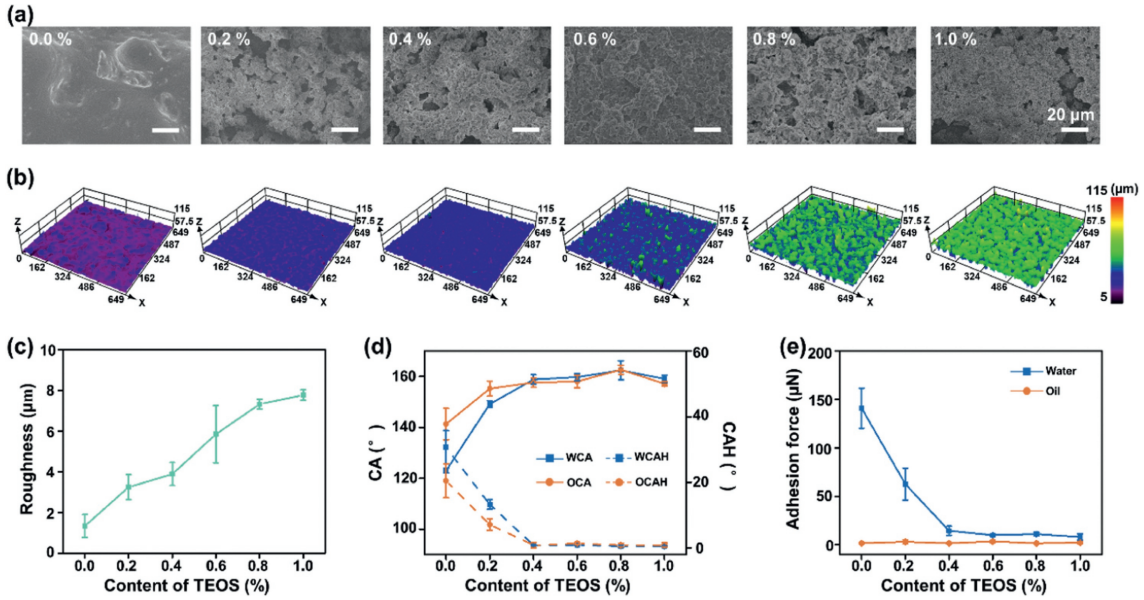

Fig. 2. Influence of TEOS content on the morphology and wetting of the SAB coating. (a) SEM images of the SAB coating with TEOS contents varying from 0.0% to 1.0%. (b, c) AFM images and corresponding surface roughness of the SAB coating with varied TEOS contents. (d, e) The variation of CA, CAH and adhesion force of water and oil on the SAB coating with varied TEOS contents.

quickly without contaminating the surface (within 120 s). Although the water exhibited spherical on the SHB coating, the oil would adhere and spread thoroughly. The crude oil would adhere and pin on the coating with much areas polluted. As for the AL surface, all the liquid would adhere and the crude oil also retain and pin on surface, leaving much residual. Thus, the SAB coating can be readily and largely prepared by spraying technology and expect to apply to anti-waxing deposition in crude oil transportation.

To regulate the morphology and wetting properties of the SAB coating, the crucial role of the TEOS, PFDTES and MMT were mainly explored from the aspects of the surface roughness, wettability and adhesion force. For TEOS, the surface roughness of the coating would increase from 1.3 ± 0.6 μm to 7.8 ± 0.2 μm with the increase of TEOS contents (Figs. 2a-c). When the TEOS content exceeded *ca.* 0.4%, the coating would undergo an apparent change and reach superamphiphobicity, displaying extremely high water contact angle (WCA) from $123.0 \pm 0.9°$ to $158.8 \pm 1.9°$, water contact angle hysteresis (WCAH) from $30.6 \pm 5.1°$ to $0.8 \pm 0.2°$, oil contact angle (OCA) from $141.3 \pm 6.1°$ to $157.6 \pm 1.9°$ and oil contact angle hysteresis (OCAH) from $20.5 \pm 5.2°$ to $0.9 \pm 0.9°$ (Fig. 2d). In contrast, low TEOS content may not trigger the hydrolysis and the particles would prefer to agglomerate. Accordingly, the adhesion force for water also changed from 141.1 ± 20.7 μN to 8.1 ± 3.3 μN (Fig. 2e). Furthermore, the influence of the concentration of PFDTES on the SAB coating was explored in Fig. S4 (Supporting information). Low concentration of PFDTES would not also trigger sufficient hydrolytic condensation resulting in low surface roughness (1.2 ± 0.2 μm). However, excessive PFDTES addition triggered self-condensation reactions that enhanced particle connectivity and covers rough surfaces with reduced roughness (5.1 ± 1.1 μm). When the PFDTES was absent, the surface would demonstrate the amphiphilicity (WCA of $22.1 \pm 4.3°$ and OCA of $26.4 \pm 8.6°$) with high adhesion force (183.2 ± 6.1 μN for water; 121.1 ± 8.6 μN for oil). Upon adding the PFDTES, the surface changed to superamphiphobicity (WCA of $161.9 \pm 2.3°$ and OCA of $158.6 \pm 1.8°$) with low adhesion force (9.3 ± 0.6 μN for water; 2.4 ± 1.4 μN for oil). Finally, the addition of MMT would undoubtedly improve surface roughness shown in Fig. S5 (Supporting information). With increasing of MMT powder from 0 mg/mL to 30 mg/mL, the surface roughness gradually enhanced from 2.35 ± 0.27 μm to 9.08 ± 0.60 μm. By introduction of MMT, the coatings would always show superamphiphobicity with CAs above 155° and CAHs below 1°. From above all, we employed the SAB coating with optimal parameter with the content of TEOS, PEDTES and MMT of 1.0%, 1.4% and 30 mg/mL respectively. To further evaluate the liquid-repellency range of the SAB coating, the wettability of various oil droplets on the coating surface were measured. As displayed in Fig. S6 (Supporting information), the SAB coating displayed excellent repellency (The OCAs, CAHs and adhesion forces were well retained above 150°, below 2°, and approximately 20 μN, respectively) toward a variety of oils, including mineral oil and hexadecane. Based on the above results, it can be concluded that the SAB coating has outstanding liquid-repellency capacity.

In general, the poor stability of the SAB coating limits their practical applications where the micro-/nanostructures can be easily damaged by abrasion or scratch. To cope with this problem, the commercial metal mesh was utilized as the protective armor for the fragile structure [43,44]. By the virtue of the spraying method, the SAB coating on the metal mesh can be easily achieved as shown in Fig. S7 (Supporting information). Here, the wear-resistance of the SAB coating was evaluated by a 1000 mesh sandpaper abrasion test with 100 g load (Fig. 3a). Even after 200 abrasion cycles, the coating still remained superhydrophobicity (WCA of $159.7° \pm 1.9°$ and WCAH of $2.1° \pm 2.3°$). While with the increase in the abrasion time, the superoleophobicity exhibited a slight decrease to OCA of $148.1° \pm 4.2°$ and OCAH of $1.8° \pm 1.5°$. The morphology of the SAB coating after 200 abrasion cycles could be observed in Fig. S7 with little change. Therefore, the influence of the sandpaper on the wetting of the SAB coating was minimal, showing the well wear-resistance property. In addition, the variation curves of the CAs and CAHs as a function of the number of tape stripping were shown in Fig. 3b. During the experiment, the adhesive surface of the tape was oriented towards the coating, and then followed by peeling off the tape vertically. The process was repeated until almost no coating debris can be observed on the tape. As depicted in Fig. 3b, an increase in tape stripping time caused little damage to the wetting of the SAB coating, maintaining the WCA of $157.6° \pm 2.8°$, WCAH of $2.8° \pm 1.8°$, OCA of $159.7° \pm 5.2°$ and OCAH of $2.4° \pm 0.5°$. The image in Fig. S7 also demonstrated the almost unchanged state of coating after test. The coating exhib-

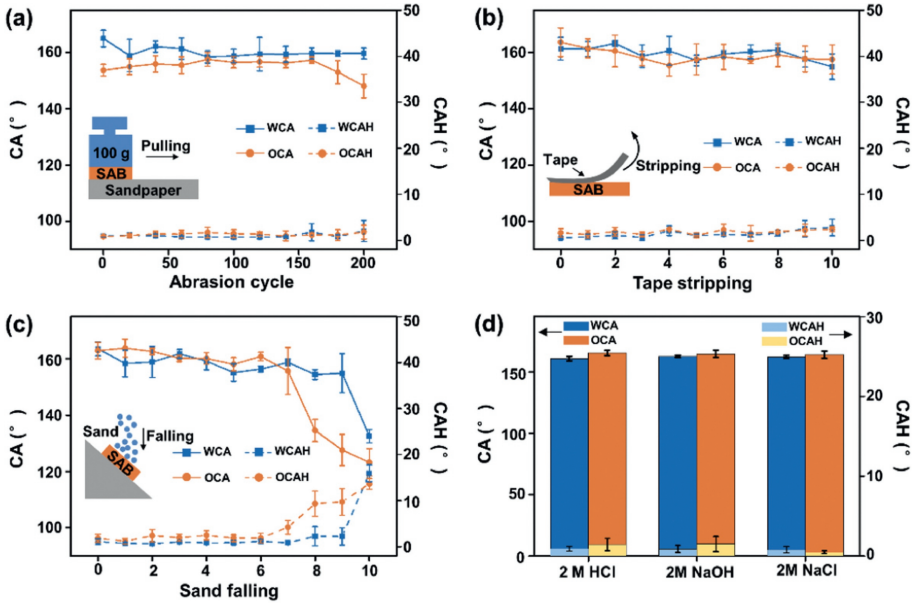

Fig. 3. The mechanical resistance and chemical stability of the SAB coating. (a) The CAs and CAHs variations of SAB coating after sandpaper abrasion cycles. (b) The relationship between CAs and CAHs with the number of tape stripping times. (c) The relationship between CAs and CAHs curves on the SAB coating with times of sand falling. (d) The CAs and CAHs of the SAB coating after immersion in 2 mol/L HCl solution, 2 mol/L NaOH solution, and 2 mol/L NaCl solution for 24 h.

ited well adhesion with a few regions removed reaching the rating 4B of the standard ASTM D3359 tape tests [45]. Such outstanding wear-resistance property could be explained by the protective metal mesh providing the micro-armor and the F-MMT micro-/nano-hierarchical fillers as secondary granules to withstand the primary abrasion at the tips of coating. Thus, the prepared SAB coating showed apparent stability and durability, substantiating its superior wearability.

The falling sand test was performed to verify the impact-resistance of SAB coatings (Fig. 3c). The coatings keeping at 45° tilting was impinged by the sand grains (10 g every time, 0.1–0.2 mm in diameter) from the height of 40 cm. Obviously, the wetting of the coating occur decreased after eight impacting times with OCA of 134.6° ± 4.0° and OCAH of 13.7° ± 1.2°. After ten impacting times, the superhydrophobicity also underwent apparent change to WCA of 132.5° ± 2.4° and WCAH of 15.9° ± 1.8°. Although the falling sand pose some damages, the coatings still remained amphiphobic, showing the hierarchical structure has certain impact-resistance. To illustrate the resistance of the SAB coating against harsh chemical environments, the coating was immersed in concentrated HCl (2 mol/L), NaOH (2 mol/L), and NaCl (2 mol/L) for 24 h, and then the CAs and CAHs were measured as shown in Fig. 3d. Regardless of the surrounding environment, CAs and CAHs were always kept above 160° and below 1°. The well chemical durability could be attributed to the presence of the air layer between liquid and the rough structure of the coating, effectively preventing corrosive liquids from penetrating the coating. In all, the obtained SAB coating possesses excellent mechanical robustness and chemical stability which is of great significance to the real-world application of the coating.

To prove the advantage of the SAB coating in anti-adhesion, the AL surface and SHB coating were utilized as control in scaling deposition and oil adsorption test. The SHB coating was prepared as the previous literature and the morphology can be seen in Fig. S8 (Supporting information) [46]. Firstly, the samples were immersed in saturated $CaCO_3$ solution for different days. Fig. 4a showed that few scale depositions could be observed on the SAB coating. Moreover, the scale mass gain (SMG) of the SAB coating was merely for 0.3 ± 0.2 mg/cm^2 as long as two weeks scaling experiment shown in Fig. 4b. In contrast, lots of scale was deposited in the AL surface and the SMG value are greatly increased with the experiment time going on up to 14.3 ± 2.3 mg/cm^2 after two weeks. Thus, compared with the AL surface, the anti-scaling efficiency could attain *ca.* 98.2%, greatly acquire the scale accumulation problem. Undoubtedly, the SHB coating also demonstrated the excellent resist scale adhesion during two-weeks test. However, from the image in the Fig. 4c, the AL surface and SHB coating were fully covered with the liquid paraffin (dyed with Sudan IV) while the SAB coating still kept the original appearance. After the oil adsorption test (Fig. 4d), we could see the SHB coating would adsorb much liquid paraffin with the oil mass gain (OMG) of 58.2 ± 4.8 mg/cm^2, which even more than the AL surface with OMG of 50.9 ± 9.7 mg/cm^2. But our SAB coating still possessed outstanding anti-oil adhesion performance with little liquid paraffin remaining (OMG of 0.7 ± 0.1 mg/cm^2). The anti-oil efficiency also could reach 98.7% compared with the control test, showing excellent oil resistance for a long service time. By feat of the air layer in the water and oil system, as a barrier layer, the SAB coating can prevent the direct contact between the scale/oil and the substrate. In addition, the low surface energy of the SAB coating (0.1 mN/m), originating from the perfluorodecyl groups, can resist common oil compared with usual SHB coatings. According to the classic nucleation theory, the SAB coating can inhibit the scale heterogeneous nucleation due to its lower surface energy and higher Gibbs energy barrier (f = 0.99) [47–49]. As a result, this SAB coating achieves a long-term anti-adhesion effect towards scale and oil by reducing the direct contact and inhibiting the interfacial scale heterogeneous nucleation.

Considering the complexity of application environments (*e.g.*, oil production and transportation), it is essential to discuss the influence of different factors, such as the scale types and oil types. Compared with the AL surface, the SAB coating always showed an extremely low SMG value regardless of scale types (*i.e.*, $CaSO_4$, $BaSO_4$ and $MgCO_3$) in Fig. 4e. Furthermore, by changing the oil type (*i.e.*, glycerol, glycol, and mineral oil), the OMG value of the SAB coating was always lower than that of the AL surface in Fig. 4f, indicating excellent oil repellence in multiple environments. The high surface energy (*ca.* 40.7 mN/m) and low Gibbs energy barrier

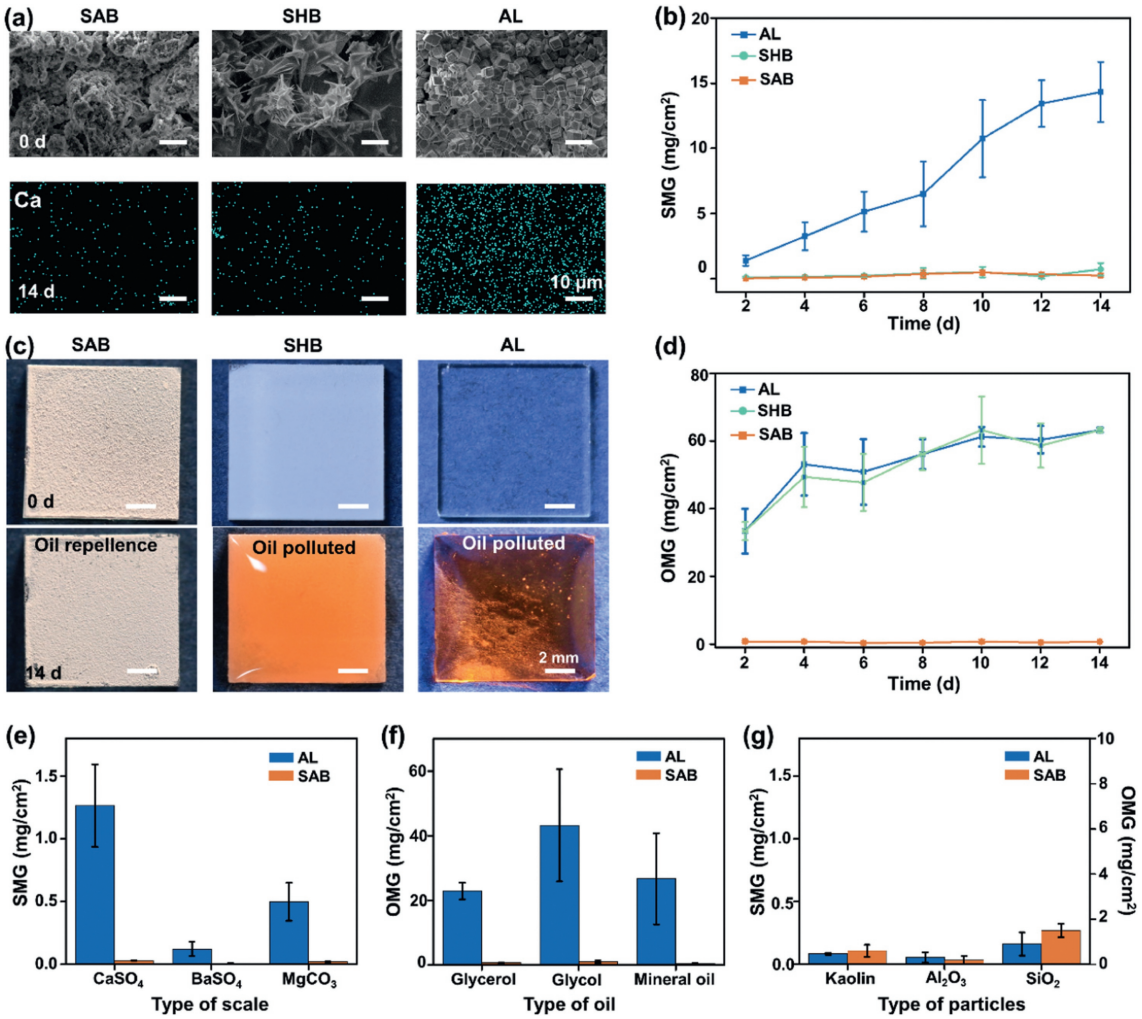

Fig. 4. Anti-adhesion towards scale and oil performance of the SAB coating. (a) The SEM and EDS images showed the scale distribution on the SAB coating, SHB coating and AL surface before and after two-weeks test. (b) The SMG change on above-mentioned substrates with testing time going by. (c) The digital images showed the appearance of above-mentioned substrates before and after oil absorption test, where the liquid paraffin is dyed with the Sudan IV. (d) The comparison of OMG change of the above-mentioned substrates during two-week test. Influence of different factors on anti-adhesion performance including varied scales (e), oils (f) and additional particles (g).

of AL surface may lead to the much scale adhesion and oil pollution [50]. By contrast, the anti-adhesion universality endowed the SAB coating with a wide range of applications. Moreover, to verify the universality of this fabrication method, different particles like kaolin, Al_2O_3, and SiO_2 were employed to form rough SAB coatings (Fig. S9 in Supporting information). In like manner, these SAB coatings exhibit excellent resistance towards scale and oil (Fig. 4g). These results showed that the essential requirements for superamphiphobicity are the hierarchical structure and low surface energy.

In summary, by regulating the wettability, our prepared SAB coating displayed the synergistic and sustainable scale and oil resistance (two weeks for 98% reduction) in various environments. Compared with the limited function of SHB and AL surfaces, the SAB coating can not only inhibit nucleation of scale crystals but also reduce the adhesion of formed scale/oil. The surface roughness and wettability of the coating was optimized by regulating the contents of TEOS, PFDTES and MMT. Moreover, the mechanical and chemical durability can be evaluated through sandpaper abrasion, tape stripping, sand falling and corrosive liquid immersing, where the SAB coatings always keep the CAs above 150° and CAHs below 2° under most tests. Moreover, the anti-adhesion universality of this coating can be revealed by varying multiple types of scale, oil, and particle, especially crude oil and wax. Therefore, this strategy provides a new idea for the design of comprehensive anti-adhesion coatings, which can be applied in complicated application environment such as oil production and transportation.

Declaration of competing interest

The authors declare that they have no known competing financial interests or personal relationships that could have appeared to influence the work reported in this paper.

Acknowledgments

This work was financially supported by the Strategic Priority Research Program of the Chinese Academy of Sciences (No. XDB 0470201), Beijing Natural Science Foundation (No. JQ23008), the National Natural Science Foundation of China (Nos. 22275203 and 22035008).

Supplementary materials

Supplementary material associated with this article can be found, in the online version, at doi:10.1016/j.cclet.2024.109623.

References

[1] A. Dhyani, J. Wang, A.K. Halvey, et al., Science 373 (2021) eaba5010.

[2] A.K. Halvey, B. Macdonald, A. Dhyani, et al., Phil. Trans. R. Soc. A 377 (2019) 20180266.
[3] J. Cao, W. Ma, W. Huang, et al., Processes 11 (2023) 1964.
[4] X. Gao, Q. Huang, X. Zhang, et al., J. Pet. Sci. Eng. 205 (2021) 108881.
[5] A. Adetunji, C. Matteo, G. Corrado, et al., Environ. Sci.: Water Res. Technol. 1 (2015) 408–425.
[6] J. Meng, S. Wang, Adv. Funct. Mater. 30 (2020) 1904796.
[7] J. Bai, X. Jin, J. Wu, Petrol. Sci. 16 (2019) 619–631.
[8] H. Yan, Q. Wu, C. Yu, et al., Adv. Mater. Interfaces 7 (2020) 2000966.
[9] Z. Li, X. Wang, H. Bai, et al., Polymers 15 (2023) 543.
[10] L. Zhang, B. Luo, K. Fu, et al., Adv. Sci. 10 (2023) 2304187.
[11] M. Zhou, L. Zhang, L. Zhong, et al., Adv. Mater. (2023) 2305322.
[12] H. Zhang, G. Zhao, S. Wu, et al., Proc. Natl. Acad. Sci. U. S. A. 118 (2021) e2100978118.
[13] Y. Chen, X. Yu, L. Chen, et al., Environ. Sci. Technol. 55 (2021) 8839–8847.
[14] F. Wu, X. Chen, S. Wang, et al., CCS Chem. (2023), doi:10.31635/ccschem.023.202302731.
[15] S. Liu, J. Lin, Q. Chen, et al., Macromol. Mater. Eng. 306 (2021) 2100242.
[16] W. Zhang, Z. Shi, F. Zhang, et al., Adv. Mater. 25 (2013) 2071–2076.
[17] W. Jie, Z. Jiale, Z. Rui, et al., Vacuum 210 (2023) 111862.
[18] Y. Li, Z. Cui, G. Li, et al., Adv. Funct. Mater. 32 (2022) 2201035.
[19] Z. Liu, L. Ren, B. Zhang, et al., Chem. Eng. J. 451 (2023) 138693.
[20] Z. Liu, C. Zhang, J. Jing, et al., Chem. Eng. J. 436 (2022) 135273.
[21] X. Yao, W. Lin, M. Wang, et al., Small 18 (2022) 2203615.
[22] X. Wang, Y. Pan, H. Yuan, et al., Chin. Chem. Lett. 31 (2020) 365–369.
[23] Z. Zhu, L. Zhong, Y. Wang, et al., Chin. Chem. Lett. 31 (2020) 2619–2622.
[24] F. Chen, Y. Wang, Y. Tian, et al., Chem. Soc. Rev. 51 (2022) 8476–8583.
[25] L. Chen, S. Huang, R.H.A. Ras, et al., Nat. Rev. Chem. 7 (2023) 123–137.
[26] X. Zhao, J. Wei, B. Li, et al., J. Colloid Interface Sci. 575 (2020) 140–149.
[27] D. Zhang, G. Wu, H. Li, et al., Chem. Eng. J. 406 (2020) 126753.
[28] J. Peng, S. Yuan, H. Geng, et al., Chem. Eng. J. 428 (2021) 131162.
[29] Z. Dai, M. Lei, S. Ding, et al., Exploration (2023). doi: 10.1002/EXP.20230046.
[30] P. Ge, S. Wang, J. Zhang, et al., Mater. Horiz. 7 (2020) 2566–2595.
[31] H. Liu, Y. Wang, J. Huang, et al., Adv. Funct. Mater. 28 (2018) 1707415.
[32] J. Ai, Z. Guo, Chem. Commun. 55 (2019) 10820–10843.
[33] N.A. Jarad, H. Imran, S.M. Imani, et al., Adv. Mater. Technol. 7 (2022) 2101702.
[34] Y. Zheng, J. Cui, Y. He, et al., Colloids Surf. A: Physicochem. Eng. Aspects 678 (2023) 132517.
[35] B. Li, W. Liang, B. Zhang, et al., Colloids Surf. A: Physicochem. Eng. Aspects 672 (2023) 131759.
[36] R. Yuan, S. Wu, H. Wang, et al., J. Polym. Res. 24 (2017) 59.
[37] E. AlShamaileh, A.M. Altwaiq, A. Al-Mobydeen, et al., Materials 16 (2023) 6291.
[38] M.K. Bangera, R. Kotian, S. Natarajan, et al., Polym. Compos. 43 (2022) 3626–3638.
[39] Q. Zhu, B. Li, S. Li, et al., J. Colloid Interface Sci. 540 (2019) 228–236.
[40] J. Peng, H. Geng, F. Xu, et al., Chem. Eng. J. 455 (2022) 140772.
[41] H. Li, Q. Jin, H. Li, et al., Adv. Funct. Mater. 34 (2023) 20239684.
[42] W. Si, Z. Guo, Adv. Colloid Interface Sci. 310 (2022) 102797.
[43] W. Zhang, D. Wang, Z. Sun, et al., Chem. Soc. Rev. 50 (2021) 4031–4061.
[44] D. Wang, Q. Sun, M. Hokkanen, et al., Nature 582 (2020) 55–59.
[45] W. Niu, G.Y. Chen, H. Xu, et al., Adv. Mater. 34 (2022) 2108232.
[46] Y. Yamauchi, M. Tenjimbayashi, S. Samitsu, et al., ACS Appl. Mater. Interfaces 11 (2019) 32381–32389.
[47] Y. Wang, R. Zhao, X. He, et al., Adv. Mater. 35 (2023) 2209696.
[48] R. Zhang, G. Azimi, ACS Appl. Mater. Interfaces 12 (2020) 42339–42347.
[49] W. Jiang, J. He, F. Xiao, et al., Ind. Eng. Chem. Res. 54 (2015) 6874–6883.
[50] A. Masoudi, P. Irajizad, N. Farokhnia, et al., ACS Appl. Mater. Interfaces 9 (2017) 21025–21033.